Filgrastim Protects the Cerebellar Cortex Against TNF-α/Bax Enhanced Apoptosis After Aluminum Toxicity in Albino Rats. Histological and Immunohistochemical Study

Heba Bayoumi[1], Mona Atya Mohamed[1], Hala Taha Shalan[2], Ebtssam Beder[3] and Enas Elgendy[1]

Original Article

[1]*Department of Histology and Cell Biology, Faculty of Medicine, Benha University, Egypt*

[2]*Department of Anatomy and Embryology, Faculty of Medicine, Ain Shams University, Egypt*

[3]*Department of Forensic Medicine and Toxicology, faculty of Veterinary Medicine, Benha University, Egypt*

ABSTRACT

Introduction: Aluminum (Al) is a strong toxicant affecting the brain neurons. Filgrastim can be a promising protective drug.
Aim of the Work: Evaluation of the neuro-alleviating role of Filgrastim on the Aluminum-induced neuronal toxicity in the cerebellar cortex.
Material and Methods: Thirty-two adult male albino rats were used in this study. The rats were divided into sets; group I (control group): rats received no drugs. Group II (Aluminum Chloride group): rats received AlCl3 at a dose of (150 mg/kg/bw; orally) dissolved in normal saline for 21 days, group III (Filgrastim +AlCl3 group): rats were trated with aluminum chloride (AlCl3) as in group II for 21 days, and were injected subcutaneously with Filgrastim at a dose of (40 µg/kg/day) for three days before AlCl3 and continued for another 21 days with AlCl3 (Filgrastim was injected 30 minutes before AlCl3). Following fixation, skulls were opened and the cerebellar cortex samples were directly handled for light and electron microscopic examination.
Results: The results of this study lead to the conclusion that Filgrastim protects the cerebellar cortex against aluminum toxicity. The histological observations showed that group II revealed extensive cerebellar cortex affection with vacuolated apoptotic cells and degenerated nerve fibers. Calbindin immunoreactivity showed a significant down-regulation (P<0.05) in Purkinje cells, while Bax and TNF-α immunoreactivity were significantly up-regulated (P < 0.05) in all layers of the cerebellar cortex. Filgrastim pre-treatment in group III improved all these histological, immunohistochemical, and ultrastructural parameters.
Conclusion: The results showed that Filgrastim can protect the cerebellar cortex from the toxic effect of Aluminium through anti-inflammatory and anti-apoptotic mechanisms.

Received: 24 December 2023, **Accepted:** 28 January 2024

Key Words: Aluminum chloride, cerebellar cortex, filgrastim, neurotoxicity.

Corresponding Author: Heba Bayoumi, MD, Department of Histology and Cell Biology, Faculty of Medicine, Benha University, Egypt, **Tel.**: +20 10 9739 0300, **E-mail:** heba.bayoumi@fmed.bu.edu.eg

ISSN: 1110-0559, Vol. 47, No. 4

INTRODUCTION

Aluminum (Al) is a common element found in soil, water, and air, and is thought to be the third most prevalent component in the earth's shell[1]. According to a significant study published by the World Health Organization (WHO), individuals are primarily exposed to aluminum through the use of cooking implements, food antacids, toothpaste, and deodorizers. In addition to occupational exposure from things like defense-related factories, cars, and weapons. Moreover, food packaging with aluminum foil and water sanitization are two common uses for soluble aluminum salts[2]. Because aluminum is so widely present, it is nearly impossible to avoid coming into contact with this metal ion[3].

There is no exact biological role known for Al, and its ion (Al3+) is known to cause health harmful effects[4]. The bioavailability of Al is the primary factor contributing to its toxicity. In biological systems, Al accumulates in many mammalian tissues like the brain, liver, kidney, and bone. Al is the most identified neurotoxic agent and its elimination half-life from the human brain is approximately 7 years[5]. The cell is the main target of the toxic effect of Al after intake and deposition in the tissues. This ion interacts with important parts of the cell such as the cytoplasmic biomolecules, plasma membrane moieties, nuclear structures, and mitochondria[6].

Since Al has been shown to have a function in the emergence of neurodegenerative and neurodevelopmental

DOI: 10.21608/ejh.2024.255554.1986

problems in addition to having a neurotoxic effect, numerous studies have been concerned with protective strategies[7].

One member of the growth factor family, granulocyte-colony stimulating factor (G-CSF), primarily promotes the development of committed progenitor cells into neutrophils and alters the distribution and functions of neutrophils in the body, so used in treating leukopenia. Numerous cell types, including neural cells, are also subject to its trophic actions[8]. Granulocyte colony stimulating factor was later used in animal stroke models. In these brain models, the preventive results of G-CSF on brain damage has been demonstrated, and positive outcomes have been achieved[9]. So, scientists are interested in G-CSF because of its unique useful effects.

While Al poisoning primarily affects the brain, its effects on the cerebellar cortex's structure have not been well studied. It is also necessary to research the usage of G-CSF as a neuroprotective medication against Al poisoning. Taking into consideration the previously mentioned information, the objective of this study was to determine the effect of AlCl3 poisoning on the microscopic organization of the cerebellar cortex and to determine whether concurrent administration of G-CSF would provide any defense.

MATERIAL AND METHODS

Animals

Thirty-two adult male albino rats, weighing between 170 and 200 grams, were used in the current study. They were acquired from the Centre of Laboratory Animals, Faculty of Veterinary Medicine, Benha University, Egypt. Earlier in the experiment, each animal was allowed to acclimatize to the lab environment for one week. During the trial, rats were housed in specialized animal cages in groups of four and fed with standard chow and tap water ad libitum. The lab temperature was (29 ± 1 °C), with (55 ± 5 %) humidity, and 12 h/12h light-dark cycles.

Ethical approval

The Institutional Animal Care Committee of Benha University, Faculty of Veterinary Medicine, Benha, Egypt, authorized all elements of this research, with an ethical approval number (BUFVTM 09-12-22).

Chemicals

- Filgrastim (recombinant human granulocyte colony-stimulating factor (rhG-CSF)): was purchased from (Sidco Company, Egypt) in the form of vial containing injectable solution.
- Aluminum chloride hexa-hydrate (AlCl3. 6H2O) was purchased from (Sd Fine -Chem Limited, Mumbai, India). It was in the form of white crystalline powder which was prepared freshly in sterile water and given orally.

Animal study plan

Later after 7 days period of adaptation, the animals were assigned into 3 sets:

Group I, (Control group= 12) rats were randomly allocated into three equal smaller groups:

- Subgroup Ia (negative control; n=4): Rats were left without interference throughout the study duration.
- Subgroup Ib (control of group II; n=4): Rats received saline (0.5ml) orally for 21 days.
- Subgroup Ic (control of group III; n=4): Rats received saline (0.5ml) s.c for three days, then saline (orally) for 21 days continued with (s.c.) saline injection.

Group II (AlCl3 group= 10): Rats treated with aluminum chloride (AlCl3) at a dose of (150 mg/kg/bw;) dissolved in normal saline and given orally by gastric tube for 21 days[10].

Group III (Filgrastim +AlCl3 group= 10): Rats received aluminum chloride (AlCl3) as in group II for 21 days, and received subcutaneous injections of Filgrastim at a dose of 40 µg/kg/day[11] three days before AlCl3 and continued for another 21 days with AlCl3. Filgrastim was injected 30 minutes before every dose of AlCl3.

Perfusion Fixation and Specimens Collection[12]

Following the completion of the drug protocol, rats in each group were fasted overnight. They received an intraperitoneal injection of sodium thiopental at a dose of 25 mg/kg to induce anesthesia[13]. Following a few minutes of anesthetic, perfusion with Ringer's for about 1 minute at a rate of approximately 5 mL/minute (the heart should continue to beat and the liver should quickly appear pale in color) was done, followed by vascular fixation with (2.5%) glutaraldehyde - (4%) paraformaldehyde solution for 10 minutes (heart should stop beating and the body should begin to stiffen). Intact brains were dissected completely without any artificial damage (to obtain intact cerebellar cortices) and placed in falcon tube containing same fixative and kept at 4Co for 2 hours.

Light Microscopic study

The right cerebellar halves were fixed in 10% formal saline for one day, washed, dehydrated with upgraded alcohol concentrations, cleared, and embedded in paraffin wax. Then, 4-5 µm sections were prepared. The sections were used for:

1. Hematoxylin and eosin (H&E) staining: to examine the histopathological changes in the different groups according to standard steps discussed previously[14]. Sections were examined and micrographs were taken by a light microscope (Olympus) conected to a camera (Panasonic model: CD-220) in the LM unit, Histology Department, Faculty of Medicine, Benha University.

2. Immunohistochemical staining: other paraffin sections were fixed on positively charged slides for immune staining for the revealing of:
    - Calbindin (Ca+2-binding protein; specific cerebellar Purkinje cells marker). The primary polyclonal rabbit antibody (Abcam, England, no: 11426 Ab, dilution 1:1200) was used. Staining pattern: cytoplasmic brown color[15].
    - Bax (apoptotic marker): The primary monoclonal antibody used was the rabbit anti-rat Bax monoclonal Ab (Sigma-Aldrich, St. Louis, Mo, USA, dilution 1:1200). Staining pattern: cytoplasmic brown color[16].
    - Tumer Necrosing Factor-alpha (TNF-α) (Neuro-inflammation marker). Goat polyclonal anti-TNFα (anti-TNFα Ab (52-B83): sc-52746, 1/100 dilution (Santa Cruz -United states). Staining pattern: cytoplasmic brown color[17].

All immunohistochemical staining steps were done according to standard method[18].

Transmission Electron Microscopy (TEM) Study[19]

Semithin and ultrathin sections preparation

Following perfusion fixation, small pieces of the left cerebellar cortices, approximately (1mm^3), were kept in a mixture of primary fixative solution (2.5% glutaraldehyde + 4% paraformaldehyde) at 4˚C for 2 hours, fixed in secondary fixative solution (1% osmium tetroxide) for 60 minutes, later dehydrated in up-grades of ethanol. Later, following transferring into a mixture of (propylene oxide & epoxy resin), the tissues were embedded in freshly prepared EPON resin mixed with acetone. Semithin sections (0.5 µm thick) were cut by ultra-microtome exposed to 1% toluidine blue stain and examined. Ultrathin sections (80-85 nm thick) were put on copper grids (3.05 mm in outer diameter) and subjected to double-staining with 2% uranyl acetate subsequently lead citrate then examined and photographed with TEM (JEOL JEM 1010; JEOL Ltd., Japan) in Tanta Electron Microscopic unit, Faculty of Medicine, Tanta University, Egypt.

Morphometric study

Immune-stained sections were photo'd using an Olympus® camera connected to an Olympus® microscope with a (0.5 X) photo adaptor, using 20X and 40X objective lens, and saved as JPG. The obtained photos were evaluated by Image-Pro Plus program version 6.0 (Media Cybernetics Inc., Bethesda, Maryland, USA). Outputs were transferred to an Excel Sheet and expressed as:

1. Integrated density of Calbindin-positive cells (X200) (measuring the integrated relation between color intensity and the area of reaction) using color mono mode.
2. The % of Bax-positive area in relation to total area (X400).
3. The % of TNF-α positive area in relation to total area (X200) using binary mode.

Two slides for each specimen were obtained, and 5 unplanned non-overlapping fields from each slide were studied.

Statistical analysis

Statistics numbers collected from the research were tabulated, analyzed, and expressed as mean ± SD of the individual groups with Statistical Package for Social Science software computer database variety 23 (SPSS, Inc., Chicago, IL, USA). One-way analysis of variance (ANOVA) was used to analyze variances between groups then Tukey's multiple comparisons test was followed. Values of p less than 0.05 were set to be the minimum criterion for statistical significance.

RESULTS

Light Microscopic Results

In this study, no mortality between rats was recorded. Outcomes of all control subgroups showed similar histological findings; so, they are represented as one group.

H & E stain (Figure 1)

Group I (control group) exhibited regular arrangement of three cerebellar cortex layers; outward molecular layer, mid Purkinje cells layer, and inward granular layer. The molecular layer displayed lightly eosinophilic neuropil with two types of neuronal cells; basket cells and stellate cells. Purkinje cells appeared large pyriform shape showing open face nucleui with a noticeable nucleoli. The Granular layer appeared as aggregations of packed granule cells with dark nuclei (Figure 1A).

Group II (AlCl3-treated group) showed pyknotic nuclei of disrupted Purkinje cells, aggregates of granule cells, and vacuolated areas involving all cortical layers. Large congested blood vessels appeared (Figure 1B).

Group III (Filgrastim + AlCl3 treated group) showed relatively some normal Purkinje cells with vesicular nuclei, while others showed shrunken pyknotic nuclei. The Molecular layer showed perinuclear haloes surrounding some cells (Figure 1C).

Toluidine blue (Figure 2)

Group I showed large Purkinje cells had light-stained nuclei and noticeable nucleoli. The cells were surrounded by light-stained Bergmann astrocytes. The granular layer showed densely crowded granule cells (Figure 2A).

Group II showed a degenerated Purkinje cell layer. Purkinje cells showed deep stained cytoplasm and ill-defined nuclei with spaces among the cells. (Figure 2B).

Group III showed re-established Purkinje cell layer. Purkinje cells appeared mostly healthy. However, some

cells were degenerated. The molecular and granular layers appeared nearly normal (Figure 2C).

Immunostaining results

Calbindin immunostaining (Figure 3)

Group I showed most Purkinje cells with strongly positive Calbindin-immune reaction (Figure 3A), whereas group II showed little Purkinje cells with somato-reduction of calbindin stain (Figure 3B). Group III showed preserved Calbindin staining in many Purkinje cells with moderate intensity (Figure 3C).

Bax immunostaining (Figure 4)

Group I showed minimal immunoreactivity for Bax protein in the 3 layers of cerebellar cortex (Figure 4A). Group II showed strong immunoreactivity for Bax protein in all cerebellar cortex layers (Figure 4B). Group III showed mild immunoreactivity for Bax protein in all cerebellar cortex layers (Figure 4C).

TNF-α immunostaining (Figure 5)

Group I showed minimal immunoreactivity for TNF-α protein in all cerebellar cortex layers (Figure 5A). Group II showed strong immunoreactivity for TNF-α protein in the different layers of the cerebellar cortex (Figure 5B). Group III showed mild immunoreactivity for TNF-α protein in the different layers of the cerebellar cortex (Figure 5C).

Transmission Electron microscopic results

Molecular cell layer (Figure 6)

Group I ultrathin section showed normal nerve axons surrounded by the compacted lamellar myelin sheaths. The axons showed mitochondria in the axoplasm (Figure 6A).

Group II ultrathin section showed multiple degenerated axons with swollen disrupted mitochondria. Some myelin sheaths showed focal splitting. Large areas of vacuolation appeared (Figure 6B).

Group III ultrathin section showed nearly normal myelinated axons displaying mitochondria (Figure 6C).

Purkinje cell layer (Figures 7,8,9)

Group I ultrathin sections showed typical histological architecture of Purkinje cell with the distinguishing large pyriform cell-body, open face nucleus, and a noticeable nucleolus. The cytoplasm showed abundant rER tubules and numerous mitochondria. (Figures 7 A,B).

Group II ultrathin sections showed Purkinje cells with irregular cell membranes, dark cytoplasm with areas of vacuolation, shrunken nuclei with increased nuclear chromatin condensation, noticeable indentation of the nuclear envelopes, dilated cisternae of Golgi swollen mitochondria, and dilated cisternae of smooth and rough endoplasmic reticulum (Figures 8 A,B).

Group III Ultrathin sections showed Purkinje cells with open face nuclei and restored their euchromatin. Mitochondria appeared nearly normal (Figure 9 A,B).

Granular cell layer (Figure 10)

Group I ultrathin section showed granule cells closely packed, containing mitochondria, normal rounded heterochromatic nuclei enclosed within thin layer of cytoplasm. Normal cerebellar islands were apparent (Figure 10A).

Group II ultrathin section showed granule cells with increased density of nuclear chromatin. Some apoptotic cells were noticed and areas of vacuolated neuropil and distorted cerebellar islands (Figure 10B).

Group III ultrathin section showed some granule cells appeared nearly normal with rounded nuclei surrounded by a slightly vacuolated rim of cytoplasm. The neuropil and the cerebellar islands in between the granule cells appeared nearly normal. Few apoptotic cells were noticed (Figure 10C).

Morphometric and statistical results

- The statistical data were symbolized in (Table 1) as well as (Histograms 1,2,,3).
- The mean integrated density of Calbindin positive cells was significantly decreased ($P<0.05$) in group II in comparison with groups I and III.
- The % of +ve area of Bax immunostaining were significantly increased ($P<0.05$) in group II in comparison with groups I and III.
- The % of +ve area of TNF-α immunostaining was significantly increased ($P<0.05$) in group II in comparison with groups I and III.

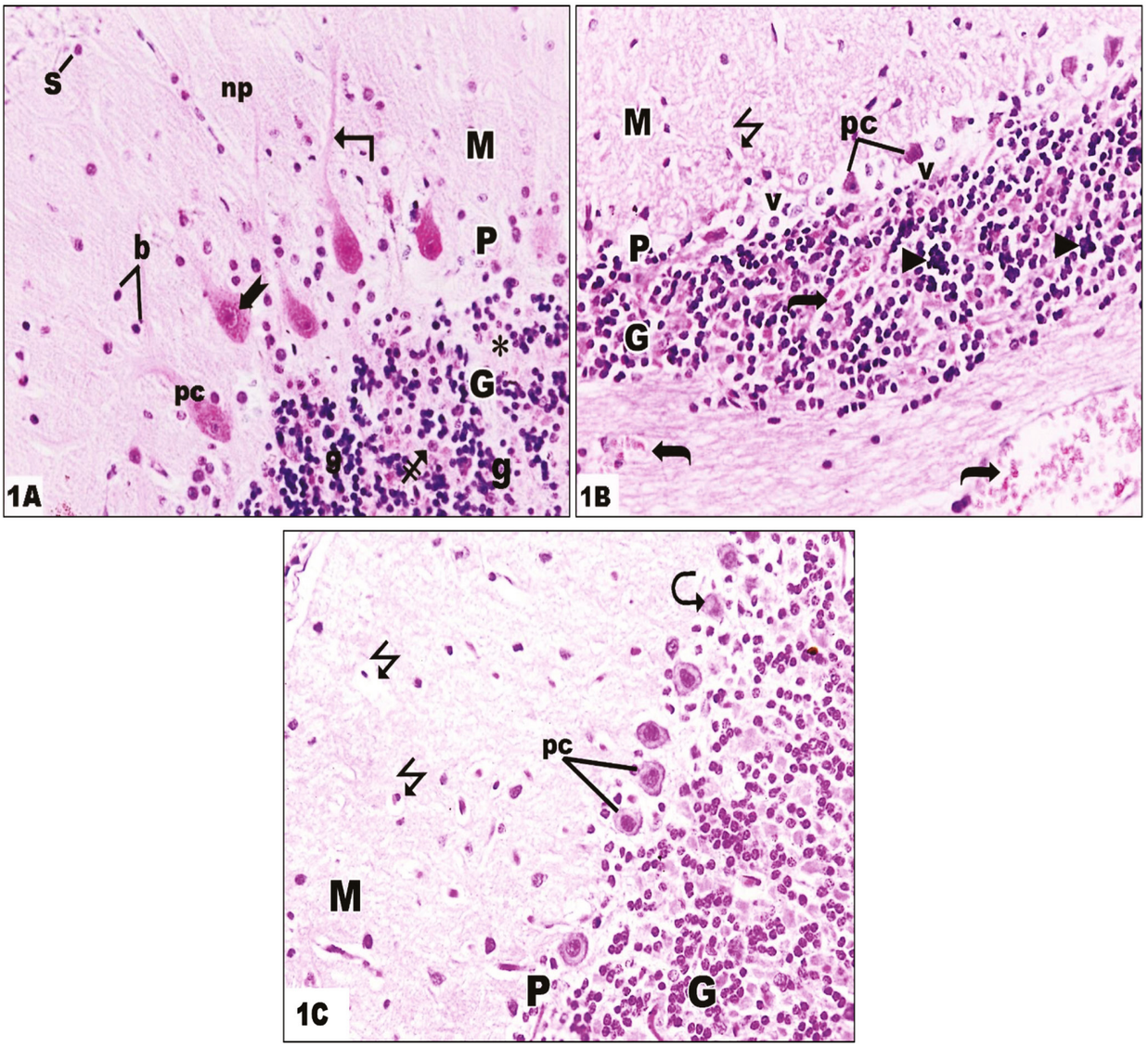

Fig. 1: cerebellar cortex representative pictures of rats stained sections with H&E, (Mag: X400) showing:
(A) Group I: Normal arrangement of three cerebellar cortex layers; outward molecular layer (M), central Purkinje cell layer (P), and inward granular layer (G). The molecular cell layer contains scattered basket cells (b) near Purkinje cells, smaller stellate cells (s) toward outside, and unmyelinated fibers "neuropil" (np). Purkinje cell layer with large "flask-shaped" cells oriented in one row (pc) showing vesicular nuclei with noticeable nucleolus (bifid arrow) and large process (angled arrow). The granular layer contains small closely packed granule cells (g) with deeply stained nuclei, more large vesicular Golgi type II cells (crossed arrow), and non-cellular pale cerebellar islands (asterisk).
(B) Group II: Most cells of the molecular layer are surrounded by perinuclear haloes (zigzag arrows). Purkinje cell layer (P) with disrupted shrunken Purkinje cells (pc) showing dark cytoplasm with pyknotic nuclei and surrounded by vacuolated areas (v). The granular cell layer (G) shows darkly stained granule cells with cellular aggregates surrounded by spaces (triangle). Notice, large congested blood vessels in the white matter of cerebellum (curved arrows).
(C) Group III: Some cells in the molecular cell layer (M) were surrounded by perinuclear haloes (zigzag arrows). Purkinje cell layer (P) shows a relatively normal appearance of some Purkinje cells having vesicular nuclei (pc), apart from a few cells with pyknotic nuclei (curved arrow). Granular cell layer (G) showing normal granule cells (g).

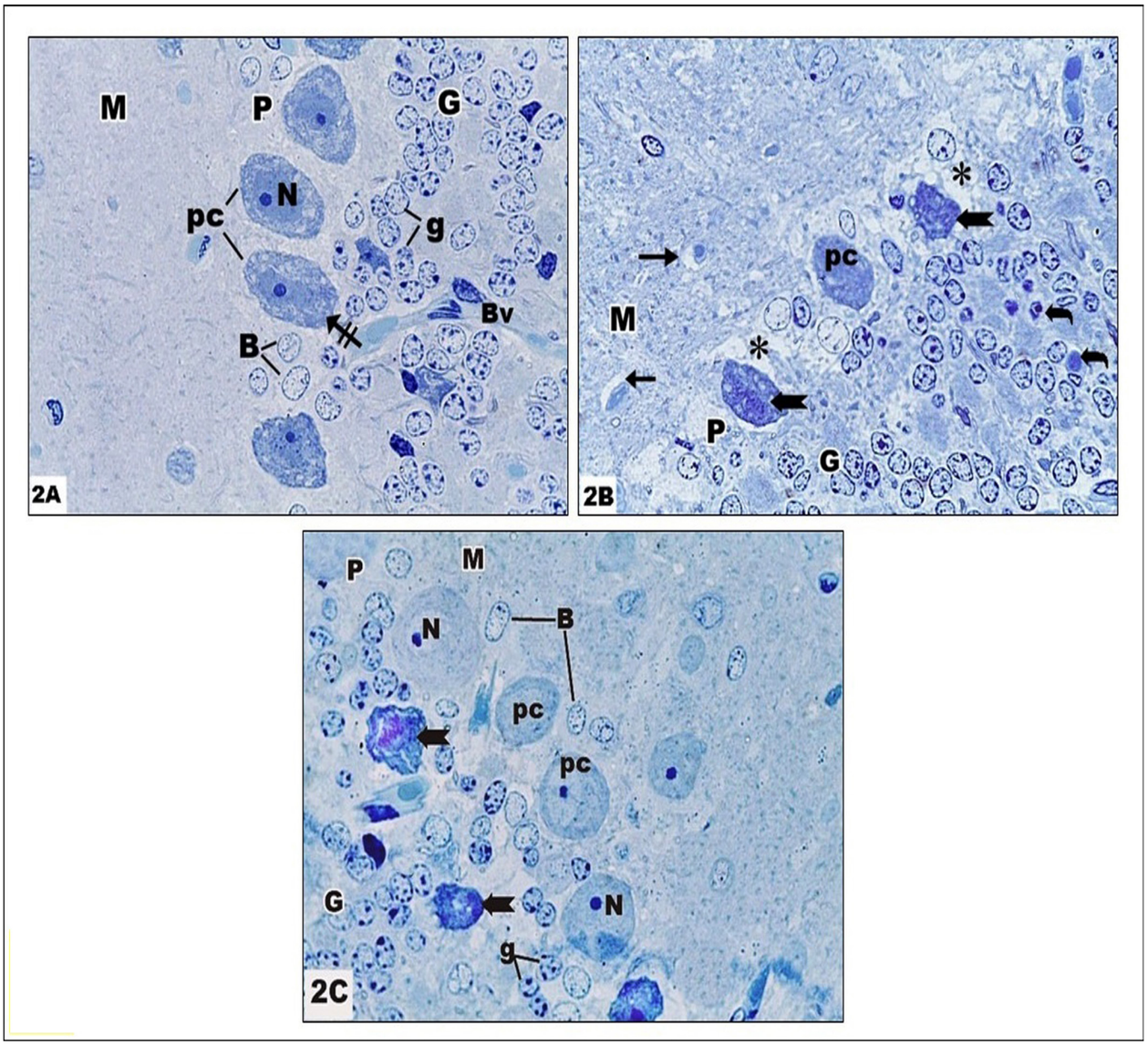

Fig. 2: Representative pictures of semi-thin sections of the cerebellar cortex of rats with toluidine blue stain (Mag: X1000) showing:
(A) Group I: Pyriform Purkinje cells (pc) with central light-stained nuclei (N), obvious nucleoli, and granular cytoplasm with Nissl,s granules (crossed arrow). The cells are encircled by pale Bergmann astrocytes (B). Granule cells (g) were colonized large nuclei and little cytoplasm. Small blood vessels appear in the field (Bv). The molecular layer (M) appeared normal.
(B) Group II: Peri-cellular haloes (arrows) appear around the cells of the molecular layer (M). Distorted Purkinje cells (pc) with dark cytoplasm (bifid arrows) and ill-defined nuclei are apparent. The surrounding neuropil shows multiple vacuoles (asterisk). The granular cell layer showed some large interneuron cells (bent arrows).
(C) Group III: Some normal Purkinje cells (pc) with vesicular nuclei (N), nucleoli, and surrounded by normal Bergmann astrocytes (B); while few cells (bifid arrows) appear deformed with dark cytoplasm and less-defined nuclei and are displaced in the granule cell layer. Granule cells (g) and molecular layer (M) are close to normal.

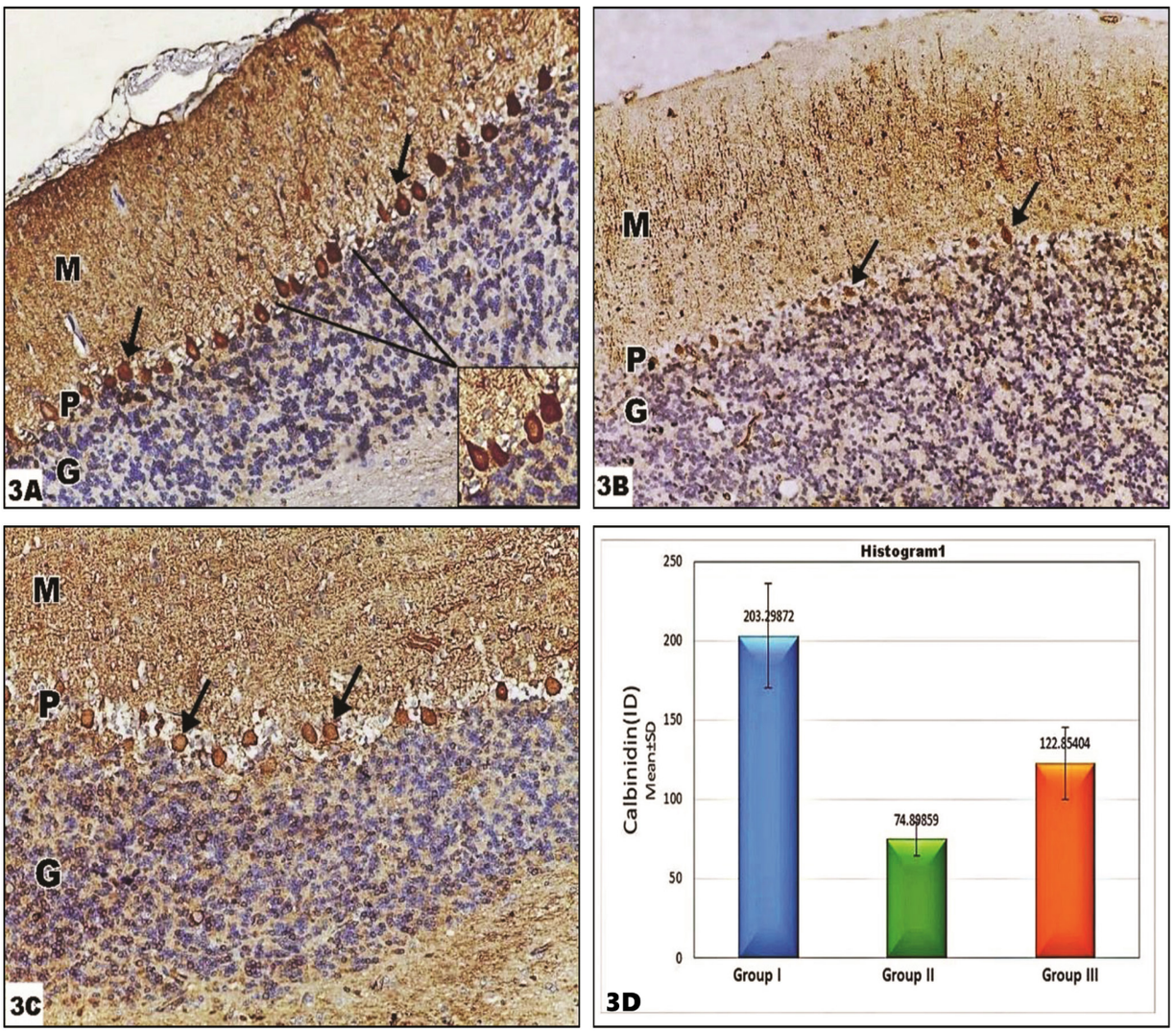

Fig. 3: Representative pictures of cerebellar cortices stained sections with Anti-Calbindin antibody of rats from experimental groups showing:
(A) Group I: Calbindin staining of cerebellar cortical layers showed high cytoplasmic expression in many Purkinje cells with strong intensity (arrows) (N.B: Inset X400). **(B)** Group II: treatment with AlCl3 showed a severe reduction in cytoplasmic calbindin expression in Purkinje cells which appeared very small compared to group I (arrows). **(C)** Group III: Many Purkinje cells with expressed moderately positive cytoplasmic immune stain for Calbindin protein (arrows). **(D)** The integrated intensity (ID) of anti-Calbindin immunoexpression was expressed as Mean±SD between experimental groups. (Anti-Calbindin; magnification: 200x)

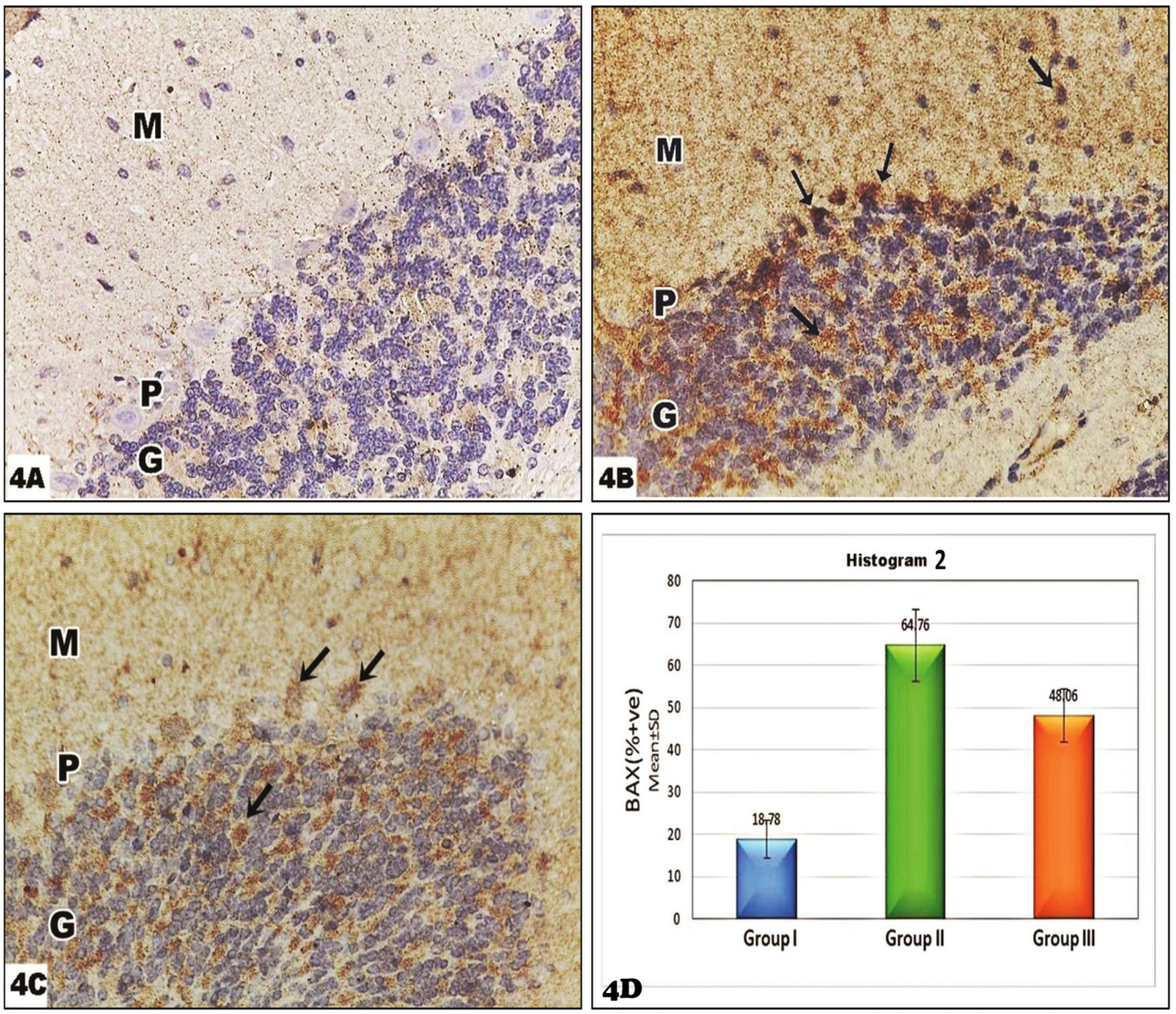

Fig. 4: Representative pictures of cerebellar cortices stained with Anti-Bax antibody of rats from experimental groups showing: **(A)** Group I: minimal cytoplasmic immune stain of Bax protein in all cerebellar cortical layers. **(B)** Group II: AlCl3 intoxicated rats showed high cytoplasmic immune stain of Bax protein (arrows), specifically apparent in Purkinje cells compared to the control group. **(C)** Group III: Filgrastim reduced the cytoplasmic immune stain of Bax protein (arrows) compared to the pathology group. **(D)**: The % of anti-Bax positive area to the total cells expressed as Mean±SD between experimental groups. (Anti-Bax; magnification: 400x)

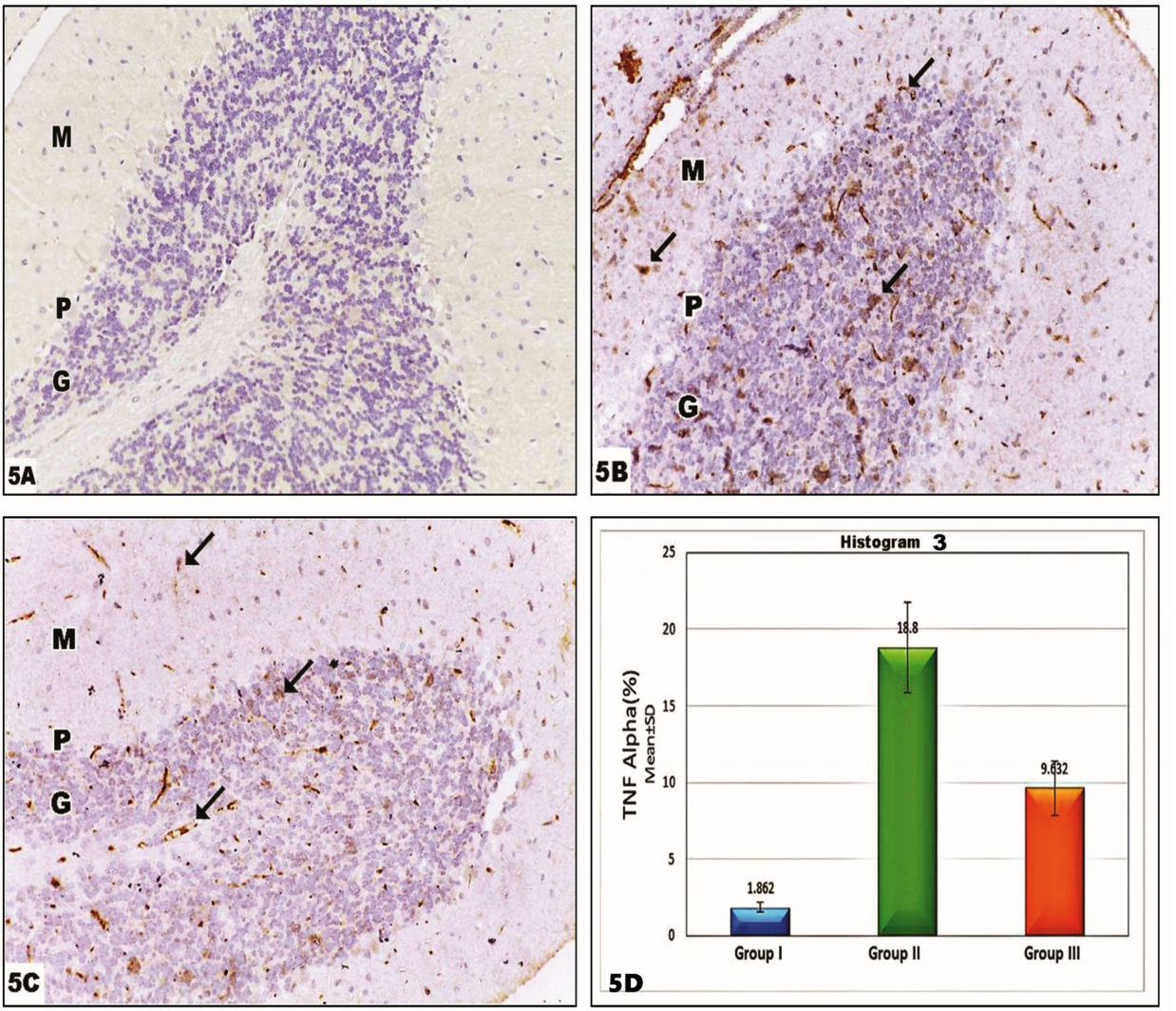

Fig. 5: Representative pictures of cerebellar cortices stained sections with Anti- TNF-α antibody of rats from experimental groups showing:
(A) Group I: Minimal immune stain of TNF-α protein in cerebellar cortical layers. **(B)** Group II: AlCl3 intoxicated rats showed strong immune stain of TNF-α protein (arrows) especially in the granular and molecular layer. **(C)** Group III: Mild immune stain of TNF-α protein (arrows) in the medulla anddsf granular layer compared to pathology group. **(D)** The area % of anti-TNF-α immunoexpression expressed as Mean±SD between experimental groups. (Anti- TNF-α; magnification: 200x)

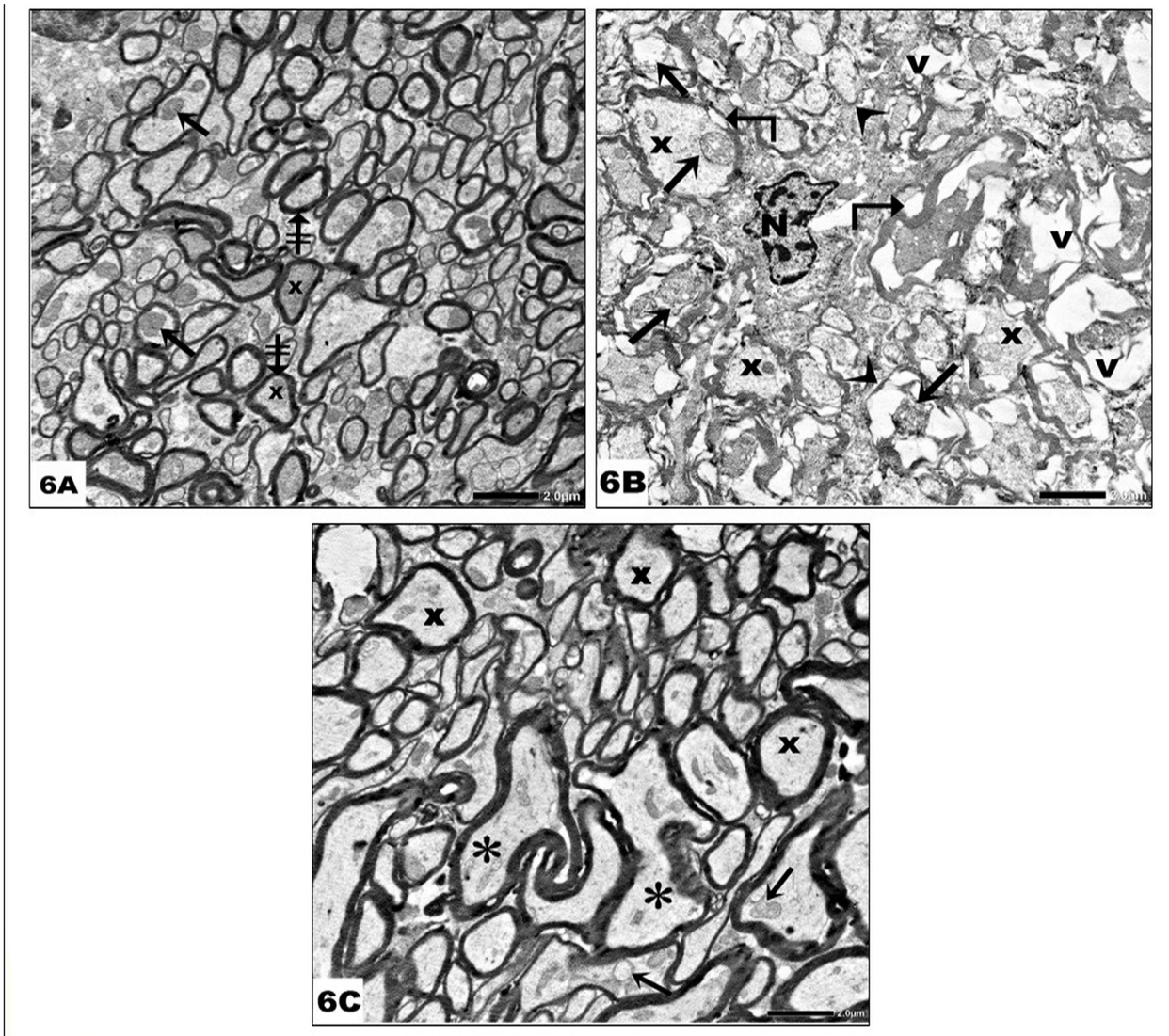

Fig. 6: Photographed molecular layer of experimental groups by transmission electron microscopy showing:
(A) Group I: cut section with almost normal nerve axons (x) surrounded by the compact myelin sheaths (crossed arrows). The axons show mitochondria (arrows) in the axoplasm. **(B)** Group II: Multiple degenerated axons (x) with swollen disrupted mitochondria (arrows). Some myelin sheaths are thin (arrowheads) and some show focal splitting (angled arrows). Areas of vacuolations can be seen in some axons (v). Notice, the nucleus astrocyte is observed (N). **(C)** Group III: Some normal myelinated axons (x) with normal myelin sheaths. The axoplasm displays mitochondria (arrows). Notice, that some fibers still with irregular outlines (asterisk). (TEM. Mag: 2000X).

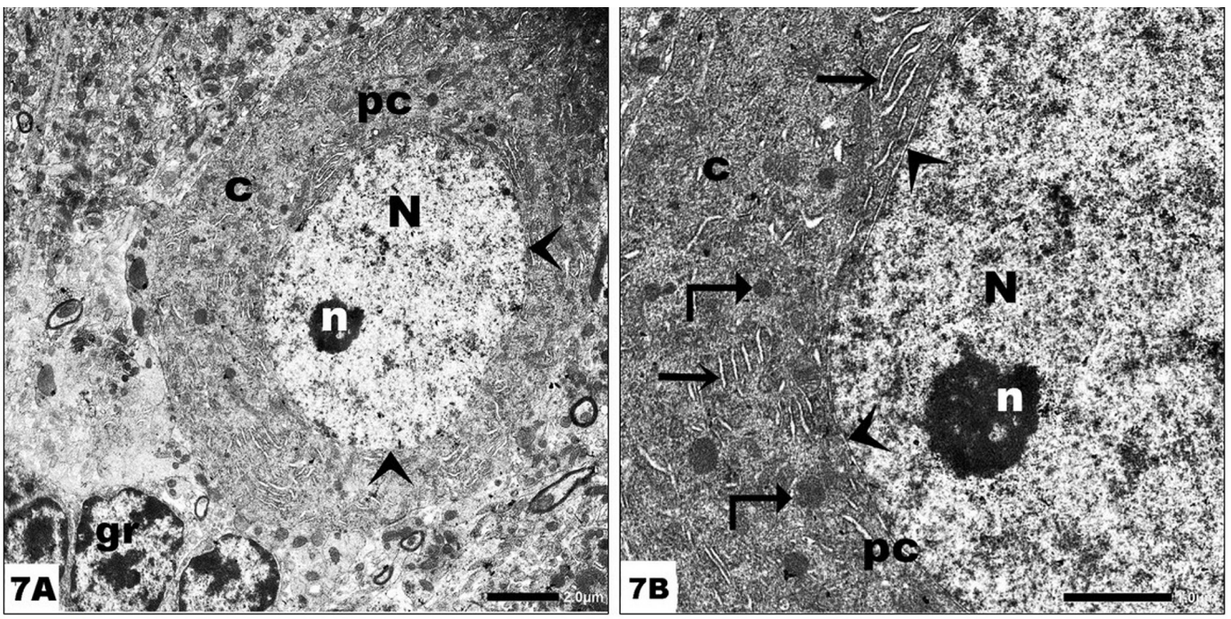

Fig. 7: Photographed Purkinje cell layer of group I by transmission electron microscopy showing: **(A)** Pyriform shape of Purkinje cell (pc) with large euchromatic nucleus (N), nucleolus (n), and nuclear envelope (arrowheads), surrounded by homogenous cytoplasm (c). Notice, some granule cells (gr). (TEM. Mag: 2000X). **(B)** Further magnification of the former photo shows large Purkinje cell (pc) with large pale stained nucleus (N), noticeable nucleolus (n), and, double-layere nuclear covering (arrowheads). The cytoplasm (c) shows mitochondria (angled arrows) and cisternae of rER (arrows). (TEM. Mag: 6000X).

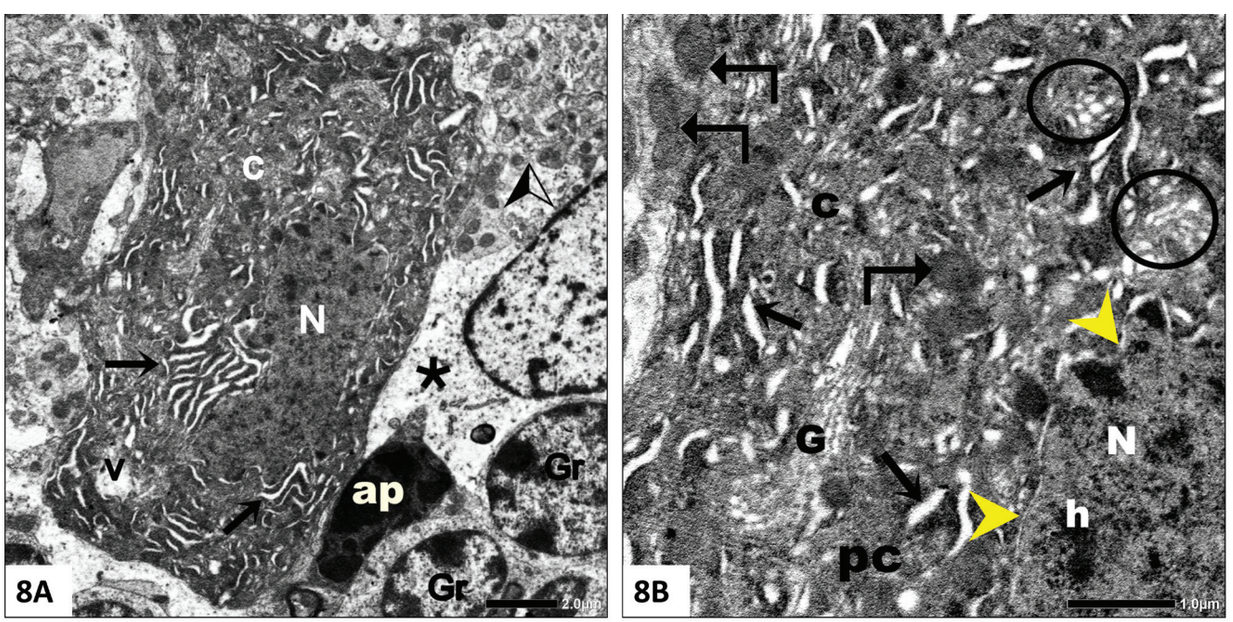

Fig. 8: Photographed Purkinje cell layer of group II by transmission electron microscopy showing: **(A)** Decreased size of Purkinje cells with irregular shrunken nucleus (N) with inapparent nucleolus, dark cytoplasm (c), some vacuolization (v) and dilated cisternae of rough endoplasmic reticulum (arrows). The surrounding area (asterisks) showing some granule cells (Gr), apoptotic microglial cell (ap), and disrupted cerebellar island (arrow head). (TEM. Mag: 2000X). **(B)** Further magnification of the former image showing Purkinje cell (pc) with part of its nucleus (N) showing areas of heterochromatin (h) and nuclear envelope indentation (yellow arrowheads). The heterogeneous cytoplasm (c) contains swollen mitochondria (angled arrow), dilated rER cisternae (arrows), dilated smooth endoplasmic reticulum (circles), and disrupted Golgi complex (G). (TEM. Mag: 6000X).

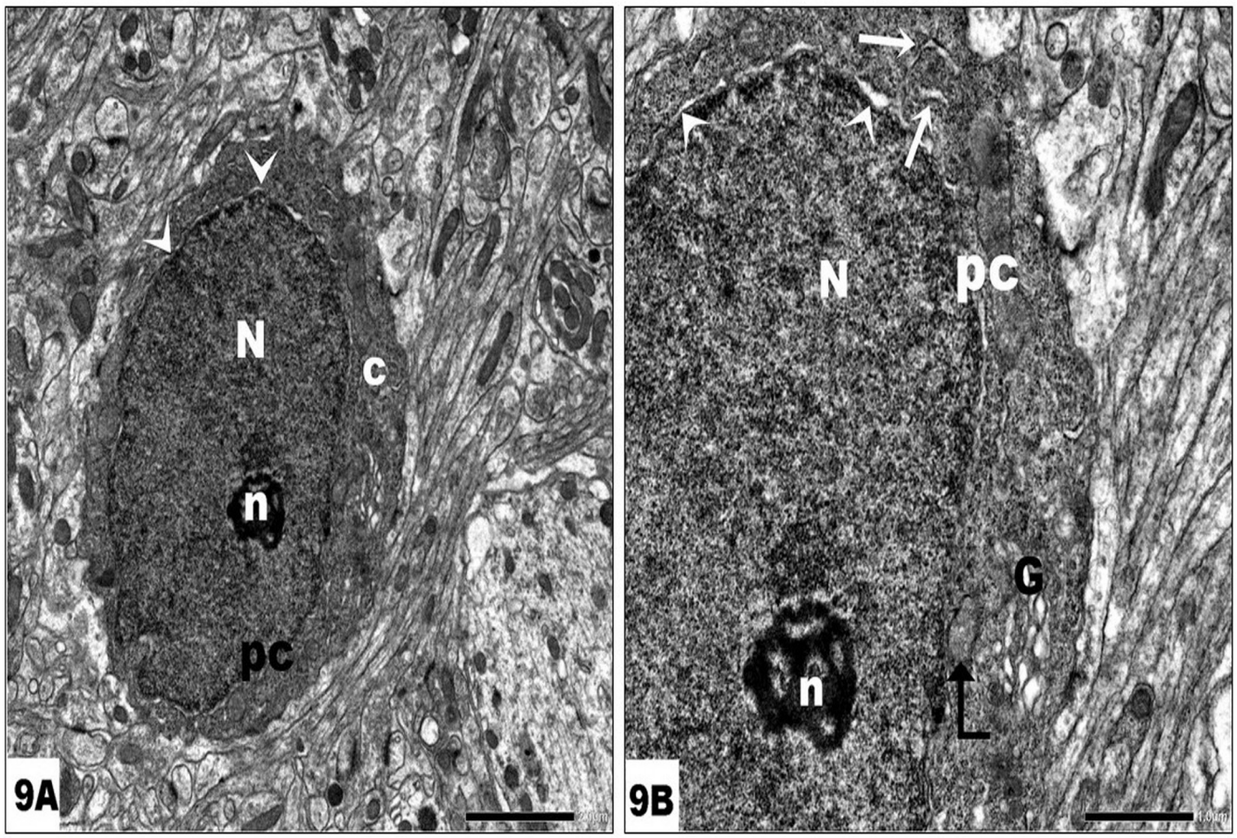

Fig. 9: Photographed Purkinje cell layer of group III by transmission electron microscopy showing: **(A)** Purkinje cell (pc) with relatively normal nucleus (N), apparent nucleolus (n), and slightly irregular nuclear envelope (arrowheads). (TEM. Mag: 2000X). **(B)** Further magnification of the former image of one Purkinje cell with part of its nucleus (N) showing nucleolus (n) and surrounded by the regular nuclear membrane (arrowheads). The cytoplasm displays nearly normal mitochondria (angled arrow), a Golgi complex with slightly dilated cisternae (G), and slightly dilated tubules of endoplasmic reticulum (arrows). (TEM. Mag: 6000X).

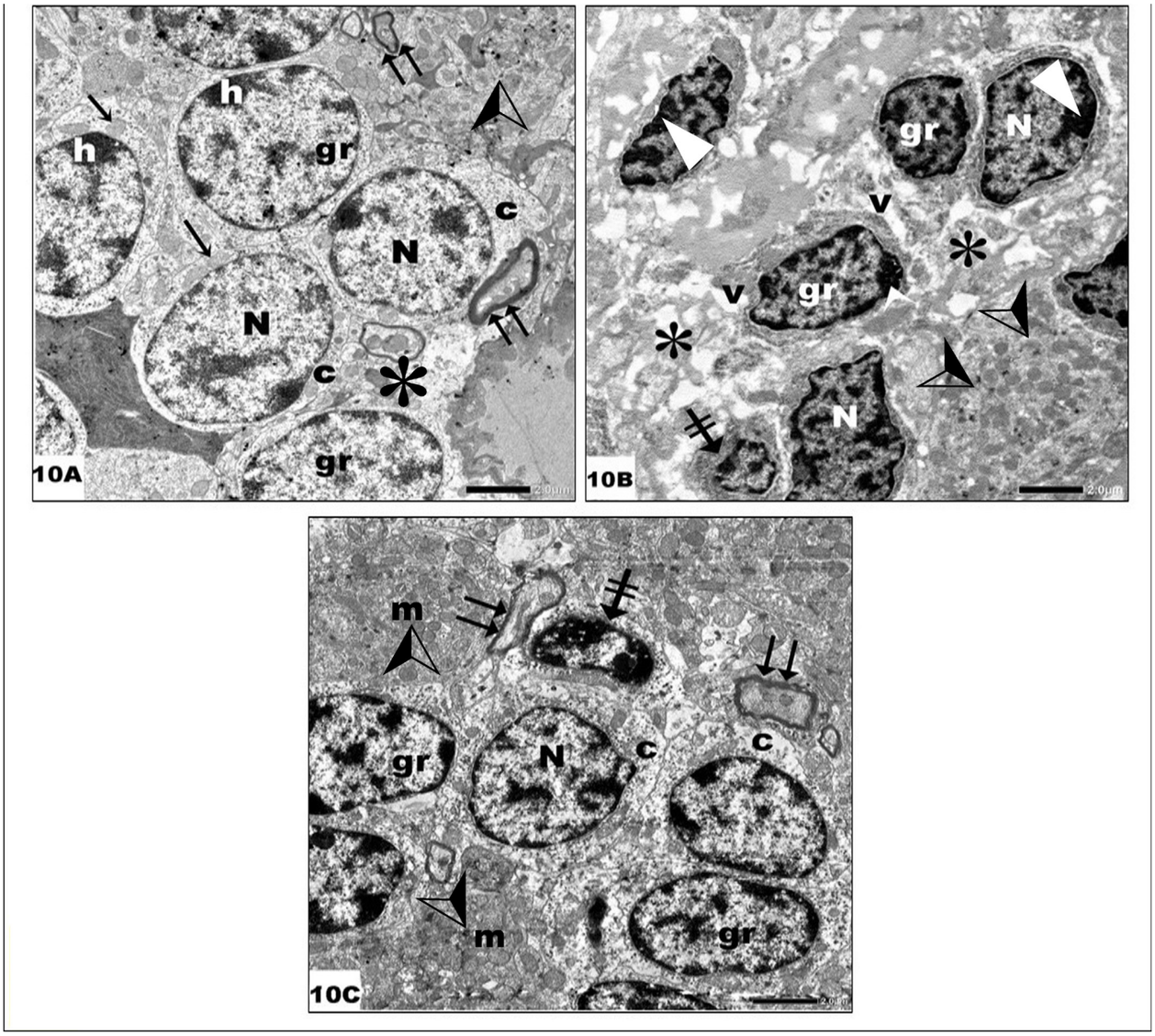

Fig. 10: Photographed granular layer of experimental groups by transmission electron microscopy showing: **(A)** Group I: Crowded granule cells (gr) with round nuclei (N) displaying areas of characteristic dense masses of chromatin (h). The nuclei are encircled by small shells of cytoplasm (c) showing mitochondria (arrows). The area between granule cells showing normal neuropil (astrikes) and normal cerebellar island (arrowhead). Notice, the myelinated nerve fiber (double arrows). **(B)** Group II: Multiple degenerated granule cells (gr) with shrunken nuclei (N) showing chromatin clumps (triangles). There is an apoptotic cell with apparently decreased size and shrunken nucleus (crossed arrow). Notice, apparently degenerated surrounding neuropil (asterisk) with vacuolated areas (v) and disrupted cerebellar island (arrowheads). **(C)** Group III: Some granule cells with rounded nuclei (N), slightly vacuolated rim of cytoplasm (c). The areas in between cells appear normal with normal two cerebellar islands (arrowheads) filled with mitochondria (m). Notice, apparently normal myelinated axons (double arrows). An apoptotic granule cell (crossed arrow) can be seen. (TEM. Mag: 2000X).

Table 1: Showing the expression and ± SD of Calbindin, Bax, and TNF-α expression of all groups.

		Group I	Group II	Group III	*P-value*
Calbindin	ID	203.30±33.26 [b,c]	74.90±10.41 [a,c]	122.85±22.88 [a,b]	<0.001*
Bax	%+ve	18.784.5[8]± [b,]c	64.76±8.48 [a,c]	48.06±6.30 [a,b]	<0.001*
TNF- α	(%) +ve	1.86±0.31 [b,c]	18.80±2.93 [a,c]	9.63±1.76 [a,b]	<0.001*

Data expressed as mean ±SD *P*: Probability *: significance <0.05 (Different letters indicate a difference in significance)
a: significance relative to Group I b: significance relative to Group II c: significance relative to Group III

DISCUSSION

The brain is the most susceptible potential target to the noxious effect of Al, and it is the most susceptible to oxidative stress due to high intensities of toxic free radicals and low levels of antioxidants after toxicity[20]. Transferrin receptors are expressed in the brain barriers. Serum transferrin binds the majority of aluminum (about 90%) following absorption allowing the passage of Al through the (BBB). Cerebrospinal fluid (CSF) contains a significantly higher concentration of Al citrate, which makes up the majority of the residual 10%. Moreover, it has been shown that some blood arteries are more prone than others to accumulate Al. These include the human brain micro-vessel endothelial cells that line the brain arteries[21]. It enters the brain but is incapable to leave, accordingly, its toxic levels in the brain progressively rises with old age. Aluminum usually forms deposits in the hippocampus and cerebellum, in addition to the cortex[22].

In the current study, the light microscopic assessment of the cerebellar cortex of AlCl3-treated group of rats revealed pyknotic nuclei of Purkinje cells with vacuolated cytoplasm, congested blood vessels, vacuolated neuropil, and more pericellular space. Purkinje cells' cytoplasm showed deep staining with ill-defined nuclei. The dark cells with increased density of cytoplasm might be clarified as one of the signs of neuronal degeneration following stressful or metabolic insult in the brain[23].

Neuropil vacuolation may result from neuronal necrosis, which degenerate resulting in expanding their processes, and presynaptic nerve terminals creating pericellular spaces[24]. Besides, the neuropil vacuoles may be resulted from swollen neuronal arborizations and presynaptic nerve terminals. Moreover, the cytoplasmic vacuoles may be linked to the swollen mitochondria[25].

The neuronal marker Calcium-binding protein Calbindin (CbD28k) is a vital marker which is greatly expressed in Purkinje cells surfaces. It has been proposed as a marker in both normal and degenerative cerebellar tissue in several species. It is of great importance in neuro-anatomy and neuropathology[26]. Such proteins play key roles in physiological mechanisms, including the regulation of intracellular Ca^{2+} concentration associated with apoptosis and cell cycle regulation[27]. High expression of Calbindin protein in cerebellar cortex Purkinje cells usually related to neuroprotective role[28]. Noticeably, features of Purkinje cell loss were evident in the present study by a significant reduction (P<0.05) in the integrated density of Purkinje cells with Calbindin immunoreactivity and a significant increase (P<0.05) in % of positive Purkinje cells of Bax immunoreactivity because of neuronal damage caused by AlCl3. Li *et al*.[29] claimed that nerve cells are known to enter into apoptosis only 2 or 3 days after injury and reach the peak after one week.

TNF-α is a pro-inflammatory cytokine that contributes to immune dysfunction and mediates inflammation, neuronal damage, and apoptosis in *vivo* and in *vitro*[30]. It is synthesized by the microglia, astrocytes, and neurons[31]. Al accumulation causes neuroinflammation by the triggering of brain microglia and astrocytes[32]. In the current study, the intoxication of rats with Aluminium significantly increased (P<0.05) area % of TNF-α expression in the layers of the cerebellar cortex. Our results fit with the previous studies.

Rajendran *et al*., Turkez *et al*., and Rahimzadeh *et al*.[33,34,35] explained that Al markedly up-regulates genes encoding pro-inflammatory signaling components especially (interleukin-1β and TNF-α). As a result, pro-inflammatory cytokines are released, which can attract leukocytes and cause them to secrete additional pro-inflammatory cytokines and other chemokines, worsening the neuro-inflammation.

These results are further supported by the examination of ultrathin sections that showed pronounced neurodegenerative changes in almost all layers of the cerebellar cortex. Marked deteriorating changes affected the myelinated neurons, where some of them displayed unbalanced alignment of their myelin coverings, whereas the others displayed focal splitting. Purkinje cells revealed shrinkage, pyknotic nuclei with heterochromatin, and dark cytoplasm with dilated tubules of rER. Granule cells also looked shrunken with irregular nuclei showing dense heterochromatin. The present results agreed with previous studies[5,36].

Keeping in view, the damages caused by AlCl3 in our study, Awad *et al* and Akanji *et al*[37,38] explained the mechanisms. Al can be attracted by brain phospholipids due to presence of negative charges, which contain polyunsaturated fatty acids and are readily attacked by reactive oxygen species (ROS) like (H2O2, O2•−, NO, and OH•) -. Al can also motivate iron-activated fat peroxidation by increasing the redox-active iron concentration. Additionally, Al causes the accumulation of H_2O_2 pool that augments the presence of more redox-active iron. This aids the enrichment of iron-related oxidative stress. This cascade leads to the production of hydroxyl free radicals

resulting in neuronal apoptosis by damaging cellular DNA and fats. ROS induces cellular harm, by amino acid residues oxidation forming protein carbonyls[39].

Since oxidative stress, inflammation, and apoptosis play a part in AlCL3-neurotoxicity, most preventive agents are anticipated to exert their effects primarily through anti-inflammatory and antioxidant properties[40]. Especially, G-CSF which is deliberated as a promising drug. In this study, we studied the effectiveness of G-CSF in the prevention of cerebellar cortex toxicity induced by AlCl3 in rats.

Notably, G-CSF and its receptor mag (G-CSFR) are broadly distributed through the adult central nervous system[41]. The expression of G-CSFR is obvious in neurons of different brain areas, such as pyramidal cells of the cerebral cortex, cerebellar Purkinje cells, cerebellar nuclei and subventricular zone (SVZ)[42], and to a lesser extent in glial cells[43]. In healthy animals, G-CSF can cross the BBB, suggesting that it may have a role in controlling physiological processes in the brain. It stimulates angiogenesis, neural regeneration, neurite growth, neuronal synapse remodeling, and neuronal role in neurological disorders[44].

G-CSF pre-treatment in group III enhanced all histological parameters. This was noticed by almost normal molecular layer and granule cells, nearly normal most of the Purkinje cells with less inter-cellular space and less vacuolated neuropil. Ultrastructural examinations supported these results. Purkinje cells showed euchromatic nuclei, normal mitochondria, and nerve fibers that appeared with normal myelin sheaths.

Noticeably, features of Purkinje cells preservation were evident in the current study by a significant increase (P<0.05) in the integrated density of Purkinje cells with Calbindin immunoreactivity and a significant decrease (P<0.05) in the % of positive Purkinje cells of Bax immunoreactivity in group III compared to group II. Moreover, a significant decrease (P<0.05) in the % area of expression of TNF-α was observed. The overall data obtained from the present results suggest that G-CSF combated neurodegeneration and neuroinflammation in group III by improving inflammation and cell survival.

Our findings were validated by other prior researchers. Exogenous G-CSF successfully penetrated the blood-brain barrier and provided brain protection in multiple experimental studies involving cerebral ischemia by inducing hematopoietic stem cell survival and mobilization into damaged brain areas. This improved neural plasticity and neuronal differentiation in addition to having antiapoptotic, angiogenic, and anti-inflammatory effects[43,45,46]. Also, Gürkan and his team concluded that G-CSF enhanced neuronal number, neurotrophic factor release, and morphological modifications, in addition to its reparative, neuroprotective, and anti-neurodegenerative properties in radiation toxicity model affecting cerebrum and cerebellum of rats[47].

Several neurodegenerative illnesses are accompanied by apoptosis, which causes neuronal death[48]. Exploring the mechanism by which G-CSF attenuates AlCl3-induced pro-apoptotic Bax in previous studies[49,50] researchers reported that during transient localized ischemia of the brain in mice, Bcl-2 protein is triggered by the activation of the G-CSF main route, which in turn suppresses caspase-3 protein to avoid apoptotic cell death. However, in a mouse model of stroke, analysis of the anti-apoptotic protein Bcl-2 revealed a rise in the Bcl-2/Bax ratios in the frontal and central regions of the G-CSF-treated group; thereby, G-CSF continues to play its neuro-protective role[51]. Moreover, a previous study showed that giving G-CSF before or after the creation of a partial nerve injury in rats had a good impact on the number of neuronal cells in the cochlear nucleus[52].

Another area of concern is that brain neuroinflammation may cause BBB injury and leukocyte migration toward the site of damage[53]. TNF-α is one of the cytokines that modulate G-CSF production[54]. Li *et al*, and Peng[55,56] found that G-CSF has a possible protective effect on nerves by antagonizing the inflammatory responses by hindering T-cell migration and infiltration to the injured brain and consequent fall of TNF-α levels via epigenetic regulation. Also, G-CSF enhances mobilization of hematopoietic stem cells from the bone marrow to the circulation, which in turn moves to the site of nerve insult by chemotactic factors secretion[57].

Our results are parallel to the results of the rat model of neonatal meningitis study[58] that provided evidence in a rat model that G-CSF can decrease the inflammatory response by lowering the quantity of cytokines released by leukocytes, including TNF-α and interleukin-1β.

However, in contrast to our results, Meuer and his team[59] injected G-CSF 24 hours prior to the induction of the Parkinson's disease rat model and observed no enhancement. Their clarification for the missing result of pre-lesion administration could be the short plasma half- life of G-CSF, and nerve cells are known to become apoptotic cells only 48-72 hours following brain injury. So, administering G-CSF before the induction of a lesion caused no observed improvement.

Regrettably, the explanations for the failure of G-CSF are still obscure. Worthy of note, there is a potential risk of G-CSF to induce thromboembolic events secondary to an inevitable leukocytosis, and consequently the risk of aggravating repeated ischemic stroke or inducing vascular insults and may impact negatively on brain inflammation[60,61].

CONCLUSION

The current study provided evidence that G-CSF protected the cerebellar cortex from AlCl3-induced toxicity. The key mechanisms involved in this potentiated protection were anti-inflammatory and anti-apoptotic effects.

CONFLICT OF INTERESTS

There are no conflicts of interest.

REFERENCES

1. Angelova I, Ivanov I, Venelinov T, Lazarova S. Occurrence of aluminum in urban water supply and sewerage systems. Int Multidiscip Sci Geo: SGEM. 2019; 19(5.1): 501–508. DOI:10.5593/sgem2019/5.1/S20.063
2. Liaquat L, Ahmad S, Sadir S, Batool Z, Khaliq S, Tabassum S, Emad S, Madiha S, Shahzad S, Haider S. Development of AD-like symptoms following co-administration of AlCl3 and D-gal in rats: A neurochemical, biochemical and behavioral study. Pak J Pharm. Sci.2017; 2(Suppl.): 647-653. PDMI: 286503335.
3. Renke G, Almeida VBP, Souza EA, Lessa S, Teixeira RL, Rocha L, Sousa PL, Starling-Soares B. Clinical Outcomes of the Deleterious Effects of Aluminum on Neuro-Cognition, Inflammation, and Health: A Review. Nutrients. 2023 May 8;15(9):2221. doi: 10.3390/nu15092221
4. Unniram Parambil AR, P K, Silswal A, Koner AL. Water-soluble optical sensors: keys to detect aluminium in biological environment. RSC Adv. (2022); 12(22):13950-13970. doi: 10.1039/d2ra01222g
5. GÖKMEN S, GÜL B. Aluminum and toxicity. Vet J. KU. (2023); 2(1):52-64 https://dergipark.org.tr/tr/pub/vetjku
6. Igbokwe IO, Igwenagu E, Igbokwe NA. Aluminum toxicosis: a review of toxic actions and effects. Interdiscip Toxicol. 2019; 12(2): 45-70. DOI: 10.2478/intox-2019-0007
7. Boland B, Yu WH, Corti O, Mollereau B, Henriques A, Bezard E, Pastores GM, Rubinsztein DC, Nixon RA, Duchen MR, Mallucci GR, Kroemer G, Levine B, Eskelinen EL, Mochel F, Spedding M, Louis C, Martin OR, Millan MJ. Promoting the clearance of neurotoxic proteins in neurodegenerative disorders of aging. Nat Rev Drug Discov. 2018; 17(9): 660-688. DOI: 10.1038/nrd.2018.109
8. Liu L, Liu Y, Yan X, Zhou C, Xiong X. The role of granulocyte colony-stimulating factor in breast cancer development: A review. Mol Med Rep. 2020; 21(5): 2019-2029. DOI: 10.3892/mmr.2020.11017
9. Zhou DG, Shi YH, Cui YQ. Impact of G-CSF on expressions of Egr-1 and VEGF in acute ischemic cerebral injury. Exp Ther Med. 2018; 16(3): 2313-2318. DOI: 10.3892/etm.2018.6486
10. Shaikh SA, Muthuraman A. Tocotrienol-Rich Fraction Ameliorates the Aluminium Chloride-Induced Neurovascular Dysfunction-Associated Vascular Dementia in Rats. Pharmaceuticals (Basel, Switzerland); (2023). 16(6), 828. DOI: 10.3390/ph16060828
11. Azmy, M.S., Menze, E.T., El-Naga, R.N. *et al*. Neuroprotective Effects of Filgrastim in Rotenone-Induced Parkinson's Disease in Rats: Insights into its Anti-Inflammatory, Neurotrophic, and Antiapoptotic Effects.(2018). Mol Neurobiol; 55(13): 6572–6588 DOI: 10.1007/s12035-017-0855-1
12. Ferrarese, B., Lunardi, N. Preparation of Newborn Rat Brain Tissue for Ultrastructural Morphometric Analysis of Synaptic Vesicle Distribution at Nerve Terminals. J. Vis. Exp.(2019); 148: e59694. doi: 10.3791/59694.
13. Kara A, Unal D, Simsek N, Yucel A, Yucel N, Selli J. Ultra-structural changes and apoptotic activity in the cerebellum of post-menopausal-diabetic rats: a histochemical and ultrastructural study. Gynecol Endocrinol 2014; 30(3): 226-231. DOI: 10.3109/09513590.2013.864270
14. Bancroft JD, Layton C. The hematoxylin and eosin, In: Suvarna SK, Layton C, Bancroft JD editors. Bancroft's Theory and Practice of Histological Techniques 2019; 8th edition, chapter 10, Pages 126-139. Elsevier. ISBN: 9780702068867
15. Cheng Q, Wu J, Xia Y, Cheng Q, Zhao Y, Zhu P, Zhang W, Zhang S, Zhang L, Yuan Y, Li C, Chen G, Xue B. Disruption of protein geranylgeranylation in the cerebellum causes cerebellar hypoplasia and ataxia via blocking granule cell progenitor proliferation. Mol Brain. 2023; 16(1):24. DOI: 10.1186/s13041-023-01010-4
16. Liu G, Wang T, Wang T, Song J, Zhou Z. Effects of apoptosis-related proteins caspase-3, Bax and Bcl-2 on cerebral ischemia rats. Biomed Rep. 2013; 1(6): 861-867. DOI: 10.3892/br.2013.153
17. Vlassaks E, Brudek T, Pakkenberg B, Gavilanes AWD. Cerebellar Cytokine Expression in a Rat Model for Fetal Asphyctic Preconditioning and Perinatal Asphyxia. Cerebellum. 2014; 13(4): 471–478. DOI: 10.1007/s12311-014-0559-2
18. Sanderson T, Wild G, Cull AM, Marston J, Zardin G. Immunohistochemical and immunofluorescent techniques, In Suvarna SK, Layton C, Bancroft JD. Editors. Bancroft's Theory and Practice of Histological Techniques 2019; 8th edition, Chapter 19, 337-394. Elsevier. ISBN: 978-0-7020-6864-5
19. Ayub B, Wani H, Shoukat S, Para PA, Ganguly S. Ali M. Specimen preparation for electron microscopy: an overview. J. Environ. Life Sci. 2017; 2(3): 85-88. www.imedpharm.com/journals/index.php/jels
20. Krupińska I. Aluminium Drinking Water Treatment Residuals and Their Toxic Impact on Human Health. Molecules. (2020); 25(3):641. doi: 10.3390/molecules25030641.

21. Bryliński Ł, Kostelecka K, Woliński F, Duda P, Góra J, Granat M, Flieger J, Teresiński G, Buszewicz G, Sitarz R, Baj J. Aluminium in the Human Brain: Routes of Penetration, Toxicity, and Resulting Complications. Int J Mol Sci. (2023); 24(8):7228. DOI: 10.3390/ijms24087228

22. Dey M, Singh RK. Chronic oral exposure to aluminum chloride in rats modulates molecular and functional neurotoxic markers relevant to Alzheimer's disease. Toxicol Mech Methods. 2022: 32(3):1-14. DOI: 10.1080/15376516.2022.2058898

23. Ismail OI, Rashed NA. Riboflavin attenuates tartrazine toxicity in the cerebellar cortex of adult albino rat. Sci Rep. 2022; 12(1):19346. doi: 10.1038/s41598-022-23894-3

24. Aboelwafa HR, El-Kott AF, Abd-Ella EM, Yousef HN. The Possible Neuroprotective Effect of Silymarin against Aluminum Chloride-Prompted Alzheimer 's-Like Disease in Rats. Brain Sci. 2020; 10(9): 628. 1-21. DOI: 10.3390/brainsci10090628

25. Hasan-Olive MM, Enger R, Hansson HA. Nagelhus ER, Eide PK. Pathological mitochondria in neurons and perivascular astrocytic endfeet of idiopathic normal pressure hydrocephalus patients. Fluids Barriers CNS 16, 39 (2019). Doi: https://doi.org/10.1186/s12987-019-0160-7

26. Zimatkin SM, Yemelyanchik SV. & Karnyushko OA. Calbindin Immunoreactivity in Rat Cerebral Cortex and Cerebellum Neurons. (2020). Neurosci Behav Physi 50(13); 384–387. DOI: 10.1007/s11055-020-00912-3

27. Lee JM, Kim CJ, Park JM, Song MK and Kim YJ: Effect of treadmill exercise on spatial navigation impairment associated with cerebellar Purkinje cell loss following chronic cerebral hypoperfusion (2018): Mol Med Rep. 17(6); 8121-8128. DOI: 10.3892/mmr.2018.8893

28. Abdelrahman SA, El-Shal AS, Abdelrahman AA, Saleh EZH, Mahmoud AA. Neuroprotective effects of quercetin on the cerebellum of zinc oxide nanoparticles (ZnoNps)-exposed rats. Tissue Barriers. (2023);11(3):2115273. DOI: 10.1080/21688370.2022.2115273

29. Li Y, Han F, Shi Y. Increased neuronal apoptosis in medial prefrontal cortex is accompanied with changes of Bcl-2 and Bax in a rat model of post-traumatic stress disorder. J Mol Neurosci. 2013 Sep;51(1):127-37. DOI: 10.1007/s12031-013-9965-z

30. Subedi L, Lee SE, Madiha S, Gaire BP, Jin M, Yumnam S, Kim SY. Phytochemicals against TNFα-Mediated Neuroinflammatory Diseases. Int J Mol Sci. 2020;21(3):764. DOI: 10.3390/ijms21030764

31. Gąssowska-Dobrowolska M, Chlubek M, Kolasa A, Tomasiak P, Korbecki J, Skowrońska K, Tarnowski M, Masztalewicz M, Baranowska-Bosiacka I. Microglia and Astroglia-The Potential Role in Neuroinflammation Induced by Pre- and Neonatal Exposure to Lead (Pb). Int J Mol Sci. (2023);24(12):9903. DOI: 10.3390/ijms24129903

32. Martínez-Hernández MI, Acosta-Saavedra LC, Hernández-Kelly LC, Loaeza-Loaeza J, Ortega A. Microglial Activation in Metal Neurotoxicity: Impact in Neurodegenerative Diseases. Biomed Res Int. 2023(3):1-27. DOI: 10.1155/2023/7389508

33. Rajendran P, Althumairy D, Bani-Ismail M, Bekhet GM, Ahmed EA. Isoimperatorin therapeutic effect against aluminum-induced neurotoxicity in albino mice. Front Pharmacol. 2023;14: 1103940. DOI: 10.3389/fphar.2023.1103940

34. Turkez H, Yıldırım S, Sahin E, Arslan ME, Emsen B, Tozlu OO, Alak G, Ucar A, Tatar A, Hacimuftuoglu A, Keles MS, Geyikoglu F, Atamanalp M, Saruhan F, Mardinoglu A. Boron Compounds Exhibit Protective Effects against Aluminum-Induced Neurotoxicity and Genotoxicity: In *Vitro* and In *Vivo* Study. Toxics. (2022);10(8):428. DOI: 10.3390/toxics10080428

35. Rahimzadeh MR, Rahimzadeh MR, Kazemi S, Amiri RJ, Pirzadeh M, Moghadamnia AA. Aluminum Poisoning with Emphasis on Its Mechanism and Treatment of Intoxication. Emerg Med Int. 2022(3);1480553. DOI: 10.1155/2022/1480553

36. Temitayo GI, Olawande B, Emmanuel YO, Timothy AT, Kehinde O, Susan LF, Ezra L, Joseph OO. Inhibitory potentials of Cymbopogon citratus oil against aluminium-induced behavioral deficits and neuropathology in rats. Anat Cell Biol. 2020 Sep 30;53(3):342-354. DOI: 10.5115/acb.20.099

37. Awad HH, Desouky MA, Zidan A, Bassem M, Qasem A, Farouk M, AlDeab H, Fouad M, Hany C, Basem N, Nader R, Alkalleny A, Reda V, George MY. Neuromodulatory effect of vardenafil on aluminum chloride/D-galactose induced Alzheimer's disease in rats: emphasis on amyloid-beta, p-tau, PI3K/Akt/p53 pathway, endoplasmic reticulum stress, and cellular senescence. Inflammopharmacology. (2023); 31(5):2653-2673. DOI: 10.1007/s10787-023-01287-w

38. Akanji MA, Rotimi DE, Elebiyo TC, Awakan OJ, Adeyemi OS. Redox Homeostasis and Prospects for Therapeutic Targeting in Neurodegenerative Disorders. Oxid Med Cell Longev. 2021(2); 3:9971885. DOI: 10.1155/2021/9971885

39. Jadhav R, Kulkarni YA. Effects of baicalein with memantine on aluminium chloride-induced neurotoxicity in Wistar rats. Front Pharmacol. 2023; 14:1034620. DOI: 10.3389/fphar.2023.1034620

40. Skalny AV, Aschner M, Jiang Y, Gluhcheva YG, Tizabi Y, Lobinski R, Tinkov AA. Molecular mechanisms of aluminum neurotoxicity: Update on adverse effects and therapeutic strategies. Adv Neurotoxicol. 2021;5:1-34. DOI: 10.1016/bs.ant.2020.12.001

41. Link, H. Current state and future opportunities in granulocyte colony-stimulating factor (G-CSF). Support Care Cancer (2022);30(9): 7067–7077. DOI: 10.1007/s00520-022-07103-5

42. Solaroglu I, Digicaylioglu M. Hematopoietic growth factor family for stroke drug development. In Translational Stroke Research, from target selection to clinical trial. 2012: Lapchak PA, Zhang JH. Editors Part II, chapter 12; 251-277. Springer.

43. Patel AMR, Apaijai N, Chattipakorn N, Chattipakorn SC. The Protective and Reparative Role of Colony-Stimulating Factors in the Brain with Cerebral Ischemia/Reperfusion Injury. Neuroendocrinology. 2021;111(11):1029-1065. DOI: 10.1159/000512367

44. Qiu X, Ping S, Kyle M, Chin L, Zhao LR. Stem Cell Factor and Granulocyte Colony-Stimulating Factor Promote Remyelination in the Chronic Phase of Severe Traumatic Brain Injury. Cells. 2023 Feb 23;12(5):705. DOI: 10.3390/cells12050705

45. Liu XM, Feng Y, Li AM. Effect of G-CSF and TPO on HIBD in neonatal rats. Asian Pac J Trop Med. (2015); 8(2):132-136. DOI: 10.1016/S1995-7645(14)60303-5

46. Wu MY, Yiang GT, Liao WT, Tsai AP, Cheng YL, Cheng PW, Li CY, Li CJ. Current Mechanistic Concepts in Ischemia and Reperfusion Injury. Cell Physiol Biochem. 2018;46(4):1650-1667. DOI: 10.1159/000489241

47. Gürkan G, Atasoy Ö, Çini N, Sever İH, Özkul B, Yaprak G, Şirin C, Uyanıkgil Y, Kızmazoğlu C, Erdoğan MA, Erbaş O. Reparative, Neuroprotective and Anti-neurodegenerative Effects of Granulocyte Colony Stimulating Factor in Radiation-Induced Brain Injury Model. J Korean Neurosurg Soc. 2023; 66(5):511-524. DOI: 10.3340/jkns.2023.0049

48. Moujalled D, Strasser A, Liddell JR. Molecular mechanisms of cell death in neurological diseases. Cell Death Differ. 2021 Jul;28(7):2029-2044.

49. Shih RH, Lee IT, Hsieh HL, Kou YR, Yang CM. Cigarette smoke extract induces HO-1 expression in mouse cerebral vascular endothelial cells: involvement of c-Src/NADPH oxidase/PDGFR/JAK2/STAT3 pathway. J Cell Physiol. 2010;225(3):741-750. DOI: 10.1002/jcp.22270

50. Komine-Kobayashi M, Zhang N, Liu M, Tanaka R, Hara H, Osaka A, Mochizuki H, Mizuno Y, Urabe T. Neuroprotective effect of recombinant human granulocyte colony-stimulating factor in transient focal ischemia of mice. J Cereb Blood Flow Metab. 2006 Mar;26(3):402-413. DOI: 10.1038/sj.jcbfm.9600195

51. Modi J, Menzie-Suderam J, Xu H, Trujillo P, Medley K, Marshall ML, Tao R, Prentice H, Wu JY. Mode of action of granulocyte-colony stimulating factor (G-CSF) as a novel therapy for stroke in a mouse model. J Biomed Sci. 2020; 27(1):19. DOI: 10.1186/s12929-019-0597-7

52. Montibeller GR, Schackmann B, Urbschat S, Oertel JMK. Effect of granulocyte colony-stimulating factor on the cochlear nuclei after creation of a partial nerve lesion: an experimental study in rats. J Neurosurg. 2018 Jan;128(1):296-303. DOI: 10.3171/2016.10.JNS161109

53. Galea I. The blood-brain barrier in systemic infection and inflammation. Cell Mol Immunol. 2021 Nov;18(11):2489-2501. DOI: 10.1038/s41423-021-00757-x

54. Zhang DD, Zhang CY, Zhang YX, Cui HP, Jiao Chen, Wen-Zhi Ma, Jia H. G-CSF reduces loss of dopaminergic neurons by inhibiting TNF-α and IL-1β in mouse model of Parkinson's disease. Int J Neurosci. 2023;133(3):278-289. DOI: 10.1080/00207454.2021.1910259

55. Li Y, Piao X, Xu T, Zhang B, Shen X, Cheng XW, Zheng S. Granulocyte colony-stimulating factor protected against brain injury in a rat cerebral hemorrhage model by modulating inflammation. Exp Anim. 2022;71(2):193-203. DOI: 10.1538/expanim.21-0137

56. Peng, W. Retraction Note: Neuroprotective effects of G-CSF administration in microglia-mediated reactive T cell activation in *vitro*. Immunol Res 71, 286 (2023). https://doi.org/10.1007/s12026-022-09343-3

57. Wu CC, Wang IF, Chiang PM, Wang LC, Shen CJ, Tsai KJ. G-CSF-mobilized Bone Marrow Mesenchymal Stem Cells Replenish Neural Lineages in Alzheimer's Disease Mice via CXCR4/SDF-1 Chemotaxis. Mol Neurobiol. 2017;54(8):6198-6212. DOI: 10.1007/s12035-016-0122-x

58. Yang YN, Su YT, Wu PL, Yang CH, Yang YSH, Suen JL, Yang SN. Granulocyte Colony-Stimulating Factor Alleviates Bacterial-Induced Neuronal Apoptotic Damage in the Neonatal Rat Brain through Epigenetic Histone Modification. Oxid Med Cell Longev. 2018(28):1-10. DOI: 10.1155/2018/9797146

59. Meuer K, Pitzer C, Teismann P, Krüger C, Göricke B, Laage R, Lingor P, Peters K, Schlachetzki JC, Kobayashi K, Dietz GP, Weber D, Ferger B, Schäbitz WR, Bach A, Schulz JB, Bähr M, Schneider A, Weishaupt JH. Granulocyte-colony stimulating factor is neuroprotective in a model of Parkinson's disease. J Neurochem. 2006 May;97(3):675-686. DOI: 10.1111/j.1471-4159.2006.03727.x

60. Konstantis G, Tsaousi G, Pourzitaki C, Kitsikidou E, Magouliotis DE, Wiener S, Zeller AC, Willuweit K, Schmidt HH, Rashidi-Alavijeh J. Efficacy of Granulocyte Colony-Stimulating Factor in Acute on Chronic Liver Failure: A Systematic Review and Survival Meta-Analysis. J Clin Med. (2023); 12(20):6541. DOI: 10.3390/jcm12206541

61. Engelmann C, Herber A, Franke A, Bruns T, Reuken P, Schiefke I, Zipprich A, Zeuzem S, Goeser T, Canbay A, Berg C, Trebicka J, Uschner FE, Chang J, Mueller T, Aehling N, Schmelzle M, Splith K, Lammert F, Lange CM, Sarrazin C, Trautwein C, Manns M, Häussinger D, Pfeiffenberger J, Galle PR, Schmiedeknecht A, Berg T. Granulocyte-colony stimulating factor (G-CSF) to treat acute-on-chronic liver failure: A multicenter randomized trial (GRAFT study). J Hepatol. (2021); 75(6):1346-1354. DOI: 10.1016/j.jhep.2021.07.033

الملخص العربى

يحمي الفلجراستيم قشرة المخيخ من موت الخلايا المبرمج المعزز بالباكس و تي ان اف-ألفا بعد سمية الألمونيوم في الجرزان البيضاء. دراسة هستولوجية و هستوكيميائية مناعية

هبة بيومي[١]، منى عطيه[١]، هاله طه شعلان[٢]، ابتسام بدير[٣]، ايناس الجندي[١]

[١]قسم الأنسجة و بيولوجيا الخلية - كلية الطب البشري - جامعة بنها- مصر

[٢]قسم التشريح و الاجنة- كلية الطب البشري - جامعة عين شمس- مصر

[٣]قسم الطب الشرعي و السموم الاكلينيكية - كلية الطب البيطري –مشتهر- جامعة بنها- مصر

المقدمة: الألمنيوم هو سم قوي يؤثر على الخلايا العصبية في الدماغ. و يمكن أن يكون الفلجراستيم دواء وقائيًا واعدًا.
الهدف من الدراسة: تقييم دور للفلجراستيم في حماية قشرة المخيخ ضد السمية الناجمة عن الألمونيوم .
المواد والطرق المستخدمة: تم استخدام ٣٢ من ذكور الجرذان البيضاء البالغة لهذه التجربة. قسمت الجرذان إلى ثلاث مجموعات. المجموعة الأولى (الضابطة) ، المجموعة الثانية (مجموعة الالمونيوم كلورايد): تلقت الجرذان الالمونيوم كلورايد بجرعة (١٥٠ ملجم/ كجم/ اليوم) مذابا في محلول ملحي عن طريق الفم بأنبوبه المعده لمدة ٢١ يوما، المجموعة الثالثة (مجموعة الفلجراستيم + الالمونيوم كلورايد) تلقت الجرذان الالمونيوم كلورايد كما جاء في المجموعة الثانية لمدة ٢١ يوما ، وحقنت تحت الجلد بالفلجراستيم (٤٠ ميكروغرام / كجم / اليوم) لمدة ثلاثة أيام قبل الالمونيوم كلورايد و لمدة ٢١ يوم مع الألمونيوم كلورايد، على ان يحقن قبل جرعة الامونيوم كلورايد بنصف ساعه. وبعد عملية الحفظ، تم فتح الجمجمة وتمت معالجة عينات قشرة المخيخ على الفور للفحص المجهري الضوئي والإلكتروني.
النتائج: كشفت نتائج الدراسة للمجموعة الثانية عن تنكس عصبي واسع النطاق لقشرة المخيخ من الناحية النسيجية ، مع انخفاض التفاعل المناعي لبروتين الكالبيندين بشكل ملحوظ($P < ٠,٠٥$) في خلايا بيركنجي، في حين أن التفاعل المناعي لبروتين باكس و عامل نخر الورم ألفا قد تزايد في جميع طبقات قشرة المخيخ($P < ٠,٠٥$) مقارنه بالمجموعه الاولى. و قد حسنت المعالجة المسبقة بواسطة العامل المحفز لمستعمرات الخلايا المحببة في المجموعة الثالثة كل هذه التغيرات النسيجية و الاحصائية.
الاستنتاج: اشارت نتائج هذه الدراسة إلى أن الفلجراستيم يحمي قشرة المخيخ من السمية العصبية التي يسببها الألمونيوم كلورايد و يتم هذا التأثير العصبي جزئيا من خلال تأثيره المضاد للالتهابات و المضاد لموت الخلايا المبرمج.